Journal of Colloid and Interface Science 535 (2019) 392–399

Contents lists available at ScienceDirect

Journal of Colloid and Interface Science

journal homepage: www.elsevier.com/locate/jcis

Regular Article

One-pot fabrication of Nitrogen-doped graphene supported binary palladium-sliver nanocapsules enable efficient ethylene glycol electrocatalysis

Chunyang Zhai [a,e], Jiayue Hu [a], Lixi Zeng [b,*], Nianqing Fu [c,*], Yukou Du [d], Mingshan Zhu [b,*]

[a] School of Materials Science and Chemical Engineering, Ningbo University, Ningbo 315211, PR China
[b] Guangdong Key Laboratory of Environmental Pollution and Health, School of Environment, Jinan University, Guangzhou 510632, PR China
[c] School of Materials Science and Engineering, South China University of Technology, Guangzhou 510640, PR China
[d] College of Chemistry, Chemical Engineering and Materials Science, Soochow University, Suzhou 215123, PR China
[e] State Key Laboratory of Photocatalysis on Energy and Environment, Fuzhou University, Fuzhou 350116, PR China

GRAPHICAL ABSTRACT

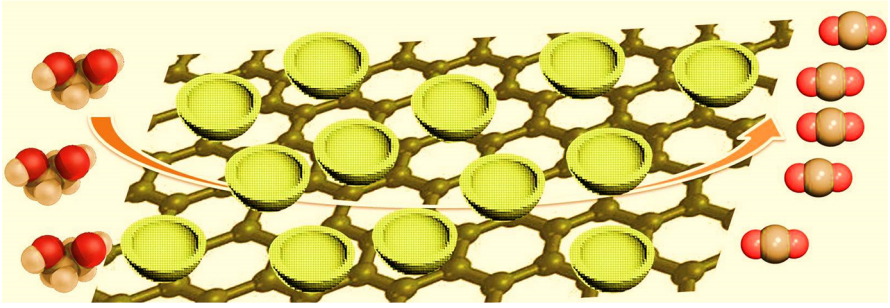

ARTICLE INFO

Article history:
Received 8 August 2018
Revised 20 September 2018
Accepted 3 October 2018
Available online 4 October 2018

Keywords:
N-doped graphene
One-pot method
PdAg nanocapsules
Fuel cells

ABSTRACT

Fuel cells hold great potential of replacing traditional fossil fuel to alleviate the energy crisis and increasing environmental concerns. Although great progresses have been achieved over decades, the sluggish reaction kinetics and poor durability of electrocatalysts in fuel cells have been the decisive bottleneck that limited their practical applications. Herein, we focus on the design and development of cost-efficient anode electrocatalysts for fuel cells and report the successful creation of an advanced class of N-doped graphene (NG) supported binary PdAg nanocapsules (PdAg NCPs). The well-defined nanocatalysts with highly open structure exhibit greatly improved electrocatalytic performances for ethylene glycol oxidation reaction (EGOR). In particular, the optimized PdAg NCPs/NG show the mass and specific activities of 6118.3 mA mg^{-1} and 13.8 mA cm^{-2}, which are 5.8 and 6.9 times larger than those of the commercial Pd/C catalysts, respectively. More importantly, such PdAg NCPs/NG can also maintain at least 500 potential cycles with limited catalytic activity attenuation, showing an advanced class of electrocatalysts for fuel cells.

1. Introduction

The rapid depletion of nonrenewable fossil fuel together with increasing energy demand in people's daily life has stimulated

* Corresponding authors.
E-mail addresses: lxzeng@jnu.edu.cn (L. Zeng), msnqfu@scut.edu.cn (N. Fu), mingshanzhu@yahoo.com (M. Zhu).

https://doi.org/10.1016/j.jcis.2018.10.003
0021-9797/

more researchers to explore environmental-friendly energy source to reduce our dependence on the immediately exhausted fossil fuel [1,2]. Direct fuel cells show great potential to serve as an ideal solution for the efficient energy conversion and storage due to their abundant advantages such as high efficiency, beneficial reliability, and low carbon emissions. Regardless of these favorable terms, the large-scale practical application of fuel cells also faces many grim challenges [3–5]. Most of all, as the central component of fuel cells, the properties of electrocatalysts can directly determine their ultimate electrochemical performances [6,7]. Currently, platinum (Pt) and Pt-based nanomaterials have been generally considered as the most efficient electrocatalysts for fuel cells reactions [8,9]. Unfortunately, the large-scale commercial application of fuel cells also faces a grand challenge due to the high cost, poor durability, as well as sluggish reaction kinetics of Pt catalyst [10–12]. Accordingly, to address these issues, designing and developing electrocatalysts with high performances yet largely reduced Pt usage have been urgently sought.

Generally, the less expensive palladium (Pd) nanomaterials have been widely considered as the most suitable candidates to replace Pt for efficient fuel cell reactions [13,14], while the commonly limited activity and poor stability of monometallic Pd have been grand problems that needed to be solved because the unfavorable electronic structure of monometallic Pd is not favorable for the electron mobility during the electrooxidation process [6]. In order to modulate the electronic structure of Pd, tremendous efforts have been made over decades. One of the most efficient strategies is to incorporate the second metal into Pd to generate the binary Pd-based alloy catalysts [15-17]. And the newly-generated Pd-based alloy catalysts can not only dramatically promote the electrocatalytic performances of catalysts, but also greatly enhance the utilization efficiency of Pd [18,19]. Moreover, after the formation of alloy, the lattice contraction is also conducive to the promotion of electrocatalytic performances [20–22].

Besides the modulation of Pd electronic structure, the predictable modification of nanostructures over surface and geometry is also another practicable approach for obtaining desirable electrocatalysts because the electrooxidation reaction commonly takes place on the surface of catalysts [23–25]. From the morphological view, the highly open nanostructure is generally considered as many advantages over the solid counterparts. This is due to the fact that the highly open nanostructures could afford a higher surface area for the electrocatalysts to contact the electrolyte and generate a beneficial electrocatalytic interface [21,26,27], which is favorable for the promotion of electrocatalytic performances.

It is also well known that the appropriate utilization of supports is beneficial for retaining the size, morphology, and dispersity of the deposited catalysts, which can thus promote the electrocatalytic performances of catalysts to a higher level. *N*-doped graphene (NG), an ideal support material, has attracted extensive attentions due to its numerous advantages, such as high conductivity and theoretical surface areas, excellent chemical stability, and fast charge transfer rate [28–31]. Moreover, the doped nitrogen element in the NG has also been demonstrated to not only modulate the electrochemical properties to effectively afford multidirectional transfer routes, but also facilitate the dispersion of deposited catalysts [32,33].

Inspired by these concepts, we herein demonstrated a facile one-pot method for the construction of capsule-like PdAg nanocatalysts that distributed on the surface of NG uniformly. Such highly open structure not only enhances the surface active areas to effectively improve the atom utilization of Pd but also benefits for the generation of ideal electrocatalytic interface, where the PdAg NCPs/NG show largely improved electrocatalytic performances for EGOR, much superior to those of Pd/C and PdAg NCPs. Moreover, the successful introduction of NG is also favorable for the promotion of long-term stability of PdAg NCPs, which can sustain for at least 500 potential sweeps with limited activity decay, showing us an advanced class of electrocatalysts for fuel cell reactions.

2. Experimental section

2.1. Chemicals and materials

Potassium hydroxide (KOH, AR), silver nitrate ($AgNO_3$, 99%), polyvinyl pyrrolidone (PVP, 8000 K), H_2PdCl_4 solution (22.6 mM), ascorbic acid (AA, 99%), ethylene glycol (EG, AR) were purchased from Sinopharm Chemical Reagent Co. Ltd, China. Commercial Pd/C (20 wt%, 2–5 nm Pd nanoparticles) was purchased from Johnson Matthey (JM) Corporation. NG (N content, 3.0–5.0 wt%) was purchased from Nanjing XFNANO Materials Tech Co., Ltd. All the chemicals were of analytical grade and have not been further purified. Secondary distilled (DI) water (18 MΩ/cm) was used in the whole process of the experiments.

2.2. Preparation of PdAg NCPs/NG and PdAg NCPs

Experimentally, the PdAg NCPs/NG was synthesized via the following procedures, 50 mg PVP, 0.9 mL H_2PdCl_4 solution (22.6 mM), and 2 mL $AgNO_3$ (10 mM) solution were added to a flask contained 10 mL secondary distilled (DI) water with rapid stirring. After the complete dissolution, a freshly prepared 4 mL AA (10 mM) solution was added dropwise to above mixture under sonicating. Subsequently, 1 mL NG (2.0 mg/mL) solution was also added dropwise into above solution to keep reacting for 1 h. The typical PdAg NCPs were prepared through the same method while in the absence of NG solution. The products were then collected via centrifugation and washing with the mixture of ethanol and acetone for three times.

2.3. Characterizations

Low-resolution energy dispersive X-ray spectroscopy (EDS) patterns was obtained by conducting on a scanning electron microscope (SEM) JEOL, JSM-6330FT. The morphology and size of the samples were analyzed by transmission electron microscope (TEM) from JEOL-2100, which operated at 100 kV instruments. Powder X-ray diffraction (PXRD) patterns were collected using an X'Pert-Pro X-ray powder diffractometer equipped with a Cu radiation source (λ = 0.15406 nm). X-ray photoelectron spectroscopy spectra (XPS) were conducted on a JEOL JPS-9010 MC spectrometer.

2.4. Electrochemical measurements

All the electrochemical measurements were performed by a typical three-electrode cell on a CHI760E electrochemical analyzer. The working electrode was a glassy-carbon electrode (GCE) (diameter: 3 mm, area: 0.07 cm^2) from the Pine Instrument. A Ag/AgCl electrode and Pt wire were used as reference and counter electrode, respectively. The GCE needs to be polished everytime before electrochemical measurements. The electrochemically active surface areas (ECSAs) were calculated based on the reduction charge of PdO with the scan rate of 50 mV s^{-1} at room temperature in 1 M KOH solution. The cyclic voltammetry (CV) for EGOR was conducted in 1 M KOH + 1 M EG solution with a rate of 50 mV s^{-1}. The 500 potential cycles CV and chronoamperometry (CA) measurement for 1 h have also been conducted to evaluate their durability. The electrochemical impedance spectroscopy (EIS) measurement of different catalysts were conducted at the potential of −0.15 V from 0.1 Hz–100 kHz. All electrochemical experiments were per-

formed at room temperature. For comparison, the Pd/C (Sigma-Aldrich, 10 wt% Pd) was used as the reference catalysts.

3. Results and discussion

The unique PdAg NCPs/NG were obtained by the simultaneous reduction of $AgNO_3$ and H_2PdCl_4 under the assistance of sonication, in which AA and PVP served as the reducing and protecting agents, respectively. Owing to the relatively low standard reduction potential of Ag^+/Ag, the newly generated Ag seeds can thus serve as the template to react with H_2PdCl_4 to generate the PdAg hollow nanostructure. As the reaction proceeded, the dissolution of Ag from the pinholes and continuous deposition of Pd atoms onto the surface result in the mesoporous nanocapsule structure.

In consideration of the unique capsule-like nanostructure and their high dispersity on the surface of NG, we herein conducted detailed characterizations such as TEM, PXRD, and XPS to thoroughly investigate their morphological and structural features. Fig. 1a–d shows the representative TEM images of the newly-generated PdAg NCPs/NG. As seen, the as-prepared PdAg nanocrystals are featured with typical capsule-like nanostructure, which are highly distributed on the surface of NG with the average diameter of 37.7 nm (Fig. S1), suggesting the successful fabrication of PdAg NCPs/NG (Fig. S2). A clear observation in the Fig. 1c and d reveals that the loaded PdAg NCPs also possesses rough surface, which includes abundant granule protuberances, being favorable for providing more surface active sites for the electrooxidation of intermediates [34–36]. To investigate its compositions, we have also conducted the SEM-EDS test, as seen in Fig. 1e, the molar ratio of Pd/Ag is calculated to be 51.2:48.8, which is consistent with the feed ratio, suggesting the complete reduction of precursors. Besides the composition investigations, we have also conducted the PXRD test to concretely gain sight into the structural information. As displayed in Fig. 1f, the typical peak at the 2θ value of around 26 is ascribed to the C (0 0 2) peak, being assigned to the NG [37]. Remarkably, the other five peaks at 40.1, 46.3, 67.8, 81.6, and 86.1 are corresponding to the (1 1 1), (2 0 0), (2 2 0), (3 1 1), and (2 2 2) crystal planes of face centered cubic (*fcc*) Pd (JCPDS No. 87-0643), respectively [38]. More interestingly, the diffraction peaks PdAg NCPs/NG, of particular is (1 1 1), which have shifted slightly to the relatively lower degree compared with pure Pd, demonstrating the successful formation of alloy phase [39]. Besides, the HRTEM has also been conducted, as seen in Fig. S3a, the interplanar spacing distance was calculated to be 0.232 nm, which was larger than that of the face-centered cubic (fcc) Pd (0.225 nm) but smaller than that of the fcc Ag (0.236 nm), indicating the generation of PdAg alloy. Furthermore, elements mappings (HAADF-STEM-EDS) and elemental line scanning profiles in Fig. S3 indicated that both Pd and Ag elements were homogeneously distributing across the whole nanocapsule, largely manifesting their alloyed nature, which was also in good accordance with the analyses of PXRD.

The XPS has also been performed to study the chemical states and compositions of the PdAg NCPs/NG because the surface atoms play crucial roles in affecting the electrocatalytic performances. As determined by XPS survey scan, the presence of Pd 3d, Ag 3d, C 1s, N 1s, and O 1s indicates the successful deposition of PdAg NCPs on the NG (Fig. 2a). The Pd 3d XPS spectrum of PdAg NCPs/NG clearly suggests that the metallic Pd is the main product with small portion of Pd^{2+} on the surface (Fig. 2b). Interestingly, compared with the binding energies of standard Pd, the Pd 3d XPS spectrum of PdAg NCPs/NG displayed an obviously positive shift, demonstrating the electron transfer from Ag to Pd, which was also another significant evidence confirming the successful generation of PdAg alloy phase [40]. Similar to Pd 3d, the metallic Ag is also the main product on the surface (Fig. 2c). Fig. 2d shows the XPS spectrum of C 1s, where the obvious peak at around 284.5 eV can be assigned to C—C bonds with the sp^2/sp^3 hybrid carbon, while the other four peaks can be reasonably assigned to the C—N, C—O, C═O, and O═C—C functional groups [41]. Fig. 2e exhibits the high-resolution N 1s spectrum, as observed, the typical N 1s spectrum can be well deconvoluted into three peaks, which are corresponding to the pyrrolic-type N, graphitic-type N, and pyridinic-type N, respectively [42]. As seen in Fig. 2f, the O 1s spectrum can be well deconvoluted into three apparent peaks presented at the binding energy of 531.4 and 532.5 eV, which are corresponding to C—O and C═O, respectively. In general, the XPS results are greatly consistent with above morphological and structural characterizations, further demonstrating the successful fabrication of NG-supported 3D PdAg NCPs and the strong interactions between PdAg NCPs and NG, both of which are propitious to boosting the electrooxidation reaction. Besides, we have also conducted the Thermogravimetric analysis (TGA) to evaluate the mass loading of PdAg NCPs on the NG. As shown in Fig. S4, the weight loss of NG before 100 °C is attributed to the evaporation of adsorbed water on the surface of NG. The weight losses at 160–250 and 480–650 °C are mainly ascribed to the pyrolysis of some oxygenated functional groups and the combustion of carbon skeleton of NG. However, after a clear observation, we can find that the PdAg NCPs/NG show smaller weight loss in comparison with the NG, and the metal loadings is assessed to be 77.6% for PdAg NCPs/NG [31].

To uncover the reaction conditions and the influence of NG on the morphology of PdAg nanocrystals, the Ag seeds and PdAg nanocrystals have also been constructed under the same conditions. As seen in Fig. S5, the as-prepared Ag seeds are the typical nanospheres with the diameter of around 35 nm, indicating that the synthesis of PdAg NCPs is a slow galvanic replacement reaction. Fig. 3a and b show the representative TEM images of the PdAg NCPs, as seen, the as-prepared PdAg nanocrystals show the typical capsule-like structure with the highly open structure and rough surface, which are similar to the PdAg NCPs that loaded on the surface of NG, indicating the introduction of NG has no influence on the morphology of the PdAg NCPs. Moreover, the SEM-EDS and PXRD patterns have also revealed that the compositions and crystal structure of PdAg NCPs are also similar to the PdAg NCPs that uniformly loaded on the surface of NG (Fig. 3c and d).

To have an intuitionistic insight of how favorable the well-defined and highly open nanostructure is, the EGOR is thus selected to evaluate the electrochemical properties of PdAg NCPs/NG. For ease of comparison, the corresponding electrochemical measurements of commercial Pd/C and PdAg NCPs have also been conducted. Fig. 4a shows the CV curves of these three types of electrocatalysts in 1 M KOH solution at the sweep rate of 50 mV s^{-1}, by which the ECSAs of different catalysts based on the coulombic charge of the Pd oxide reduction were calculated. As seen in Fig. 4b, the PdAg NCPs/NG shows an ECSA value of 44.3 $m^2 g^{-1}$, which is 4.5 $m^2 g^{-1}$ higher than that of PdAg NCPs (39.8 $m^2 g^{-1}$), and the enhancement of ECSA value of PdAg NCPs/NG can mainly be attributed to the high dispersity of PdAg NCPs on the surface of NG. The electrocatalytic activities of different catalysts were obtained by performing the CV in 1 M KOH solution containing 1 M EG at room temperature. As seen in Fig. 4c, a lower onset potential and wider potential range for PdAg NCPs/NG were showed when compared with the other electrocatalysts, indicating the superior electrocatalytic EGOR activity. To make a thorough comparison, the specific and mass activities by normalization of peak current in the forward scan with the ECSA and loading Pd mass have also been summarized. As shown in Fig. 4d, the mass activity of PdAg NCPs/NG was 6118.3 mA mg^{-1}, which was 5.8 and 1.4 times higher than those of Pd/C (1059.6 mA mg^{-1}) and PdAg NCPs (4289.2 mA mg^{-1}), respectively. With regard to specific

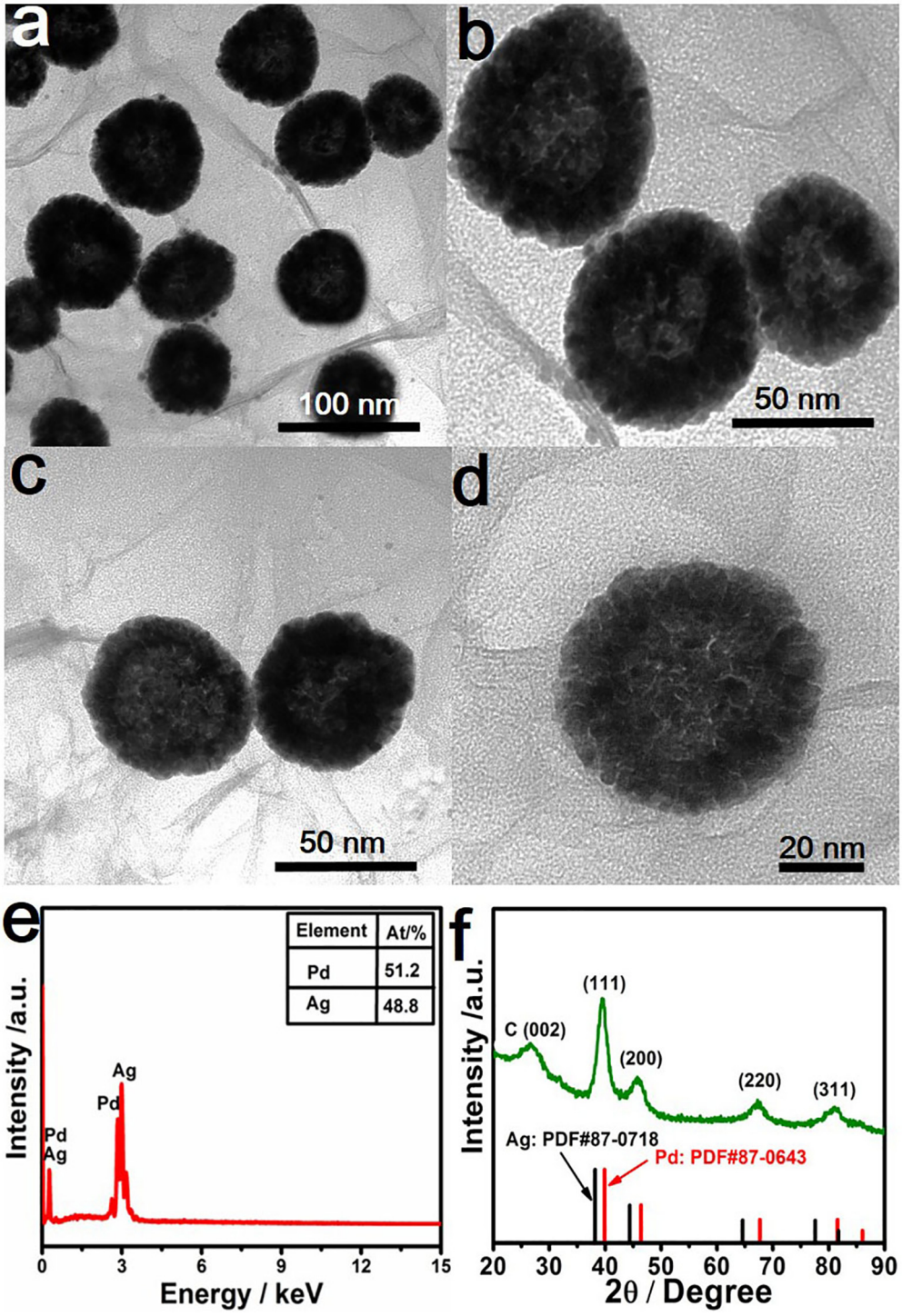

Fig. 1. (a–d) TEM images of PdAg NCPs/NG with different magnifications. (e) SEM-EDS and (f) PXRD patterns and PdAg NCPs/NG.

activity, the PdAg NCPs/NG also displayed the highest specific activity of 13.8 mA cm^{-2}, showing the superior electrocatalytic EGOR activity. More significantly, such PdAg NCPs/NG also outperformed many previously reported literatures (Table S1). To study the composition effect on the catalytic activity, we have also synthesized the other two types of PdAg NCPs/NG samples with different Pd/Ag ratios and thoroughly investigated their electrocatalytic EGOR activities. As seen in Fig. S6, the mass activities of $Pd_1Ag_{1.2}$ NCPs/NG and $Pd_1Ag_{0.5}$ NCPs/NG are calculated to be 5312.2 and 4960.3 mA mg^{-1}, respectively, both of which are much higher than those of PdAg NCPs and commercial Pt/C catalysts (Fig. S7), indicating the significant effect of NG support for the enhancement of electrocatalytic activity. However, the mass activities of these two electrocatalysts are a little lower than that of the Pd_1Ag_1 NCPs/NG, suggesting the strong composition effect on the catalytic activity.

For scrutinizing the genuine reason why PdAg NCPs/NG can display great promotion of electrocatalytic activity towards EGOR, the EIS test of different catalysts have also been conducted at the potential of -0.15 V. Generally, the diameter of semicircle arc

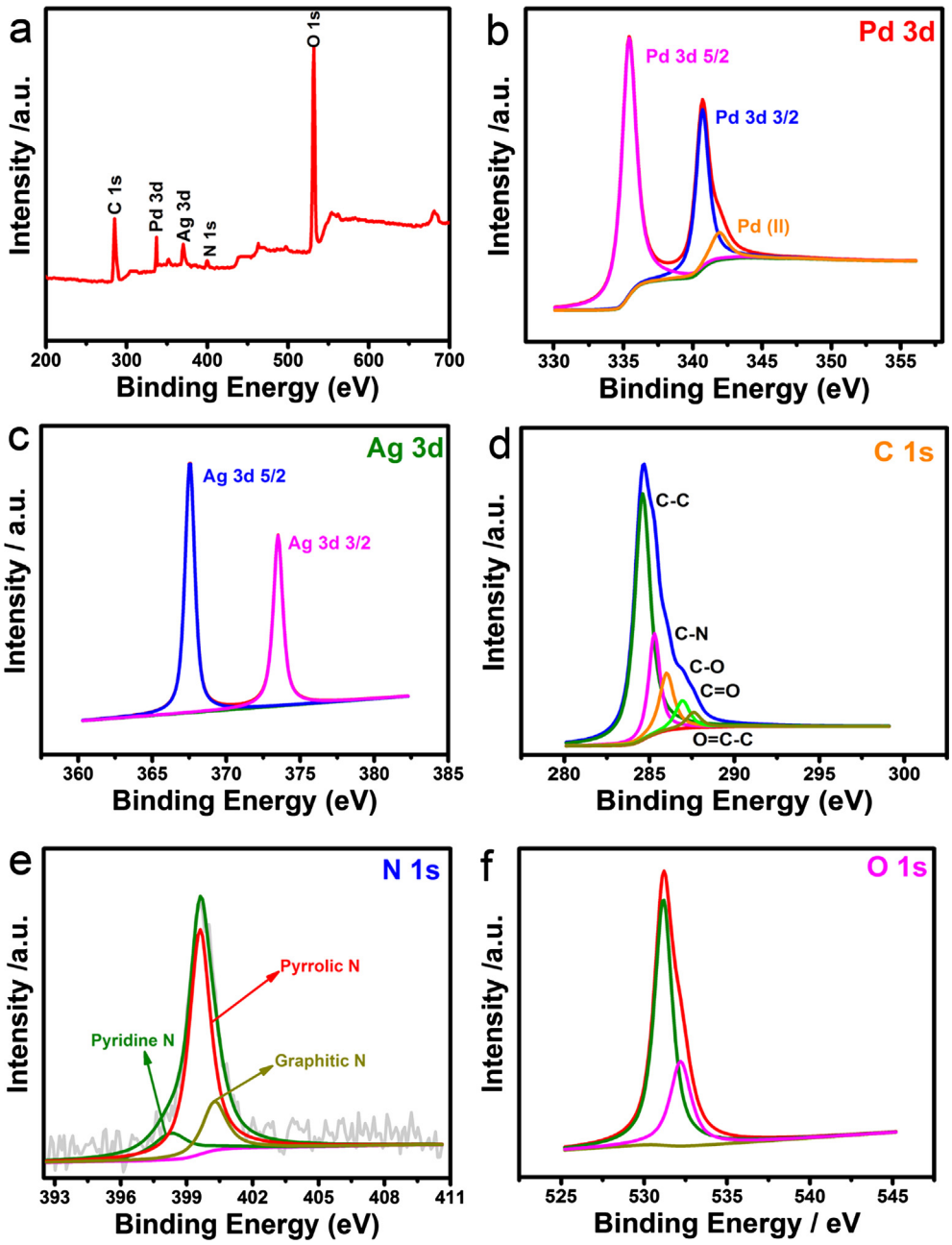

Fig. 2. XPS spectra of (a) survey scan, (b) Pd 3d, (c) Ag 3d, (d) C 1s, (e) N 1s, and (f) O 1s of PdAg NCPs/NG.

(DIA) in the Nyquist plots is crucial for evaluating the reaction kinetics of electrocatalysts, where a smaller DIA means faster reaction kinetics but lower electrochemical resistance [43,44]. As seen in Fig. 4e, the PdAg NCPs/NG displayed the smallest DIA among these electrocatalysts investigated, indicating the highest charge transfer efficiency, which was a crucial reason accounting for the great promotion of electrocatalytic activity.

Besides the electrocatalytic activity, the durability of catalyst is also crucial since the practical application of fuel cells should meet the high requirements for long-term cycle [45,46]. In this regard, the stabilities of different electrocatalysts were initially evaluated via conducting the CA at the potential of −0.1 V for 1 h 1 M KOH + 1 M EG solution. As seen in Fig. 5a, the current densities of working electrodes are all declined during the initial minute. This is mainly attributed to the unavoidable formation of Pd oxides and some CO-like intermediate species poisoning on the surface of electrode at the early stage of EGOR [22,47]. However, the decay rate for PdAg NCPs/NG is much slower than those of PdAg NCPs and commercial Pd/C. After 3600 s, the retained mass activity of PdAg NCPs/NG is 1160.1 mA mg^{-1} (Fig. 5b), which is 26.7 and 2.9 times higher than those of commercial Pd/C (42.0 mA mg^{-1}) and PdAg NCPs (404.8 mA mg^{-1}), respectively, indicating the enhanced durability of PdAg NCPs/NG relative to Pd/C and PdAg NCPs.

To further verity the superior long-term stability of PdAg NCPs/NG, the continuous 500 potential sweeps have also been conducted. As seen in Fig. S8, similar to CA measurement, the normalized current of catalysts all decay rapidly in the initial 100 cycles, which is ascribed to the formation of Pd oxides and poisoned by some poisoning intermediates. However, the PdAg NCPs/NG display remarkably superior long-term stability in comparison with the other two electrocatalysts. Impressively, after 500 potential cycles, the PdAg NCPs/NG shows only 27.5% activity loss (Fig. 6).

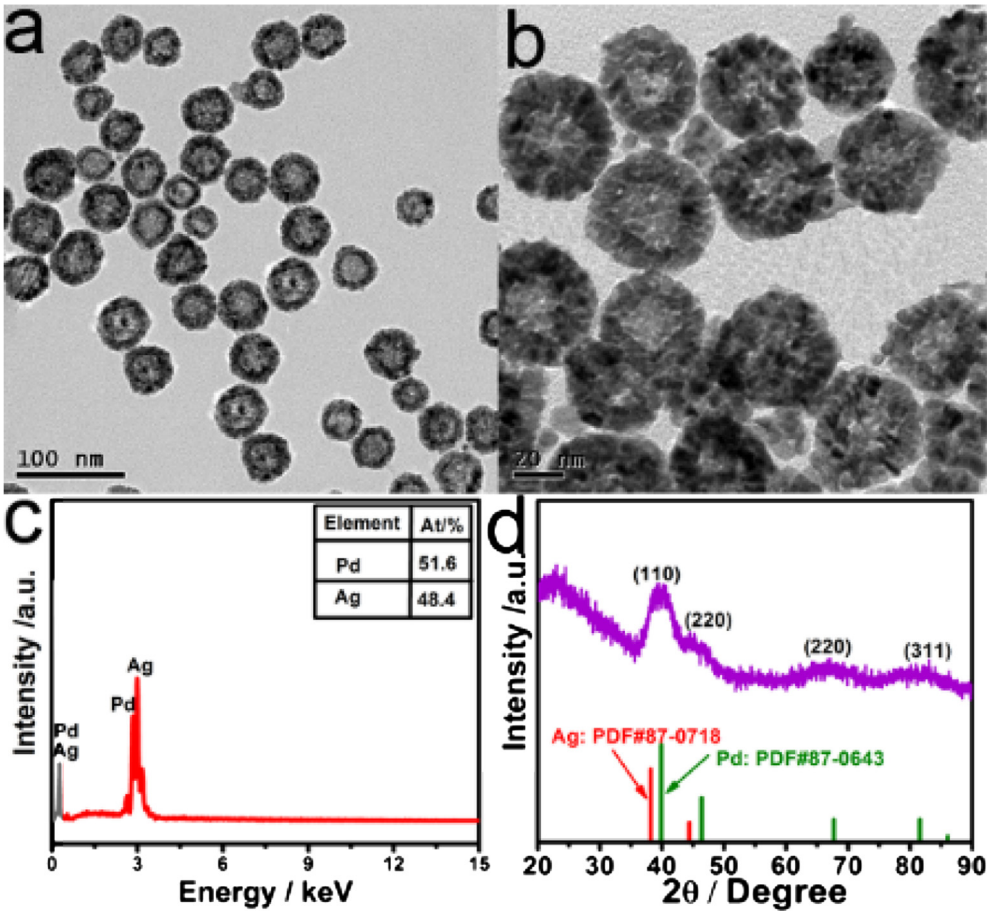

Fig. 3. (a and b) TEM images of PdAg NCPs with different magnifications. (c) SEM-EDS and (d) PXRD patterns and PdAg NCPs.

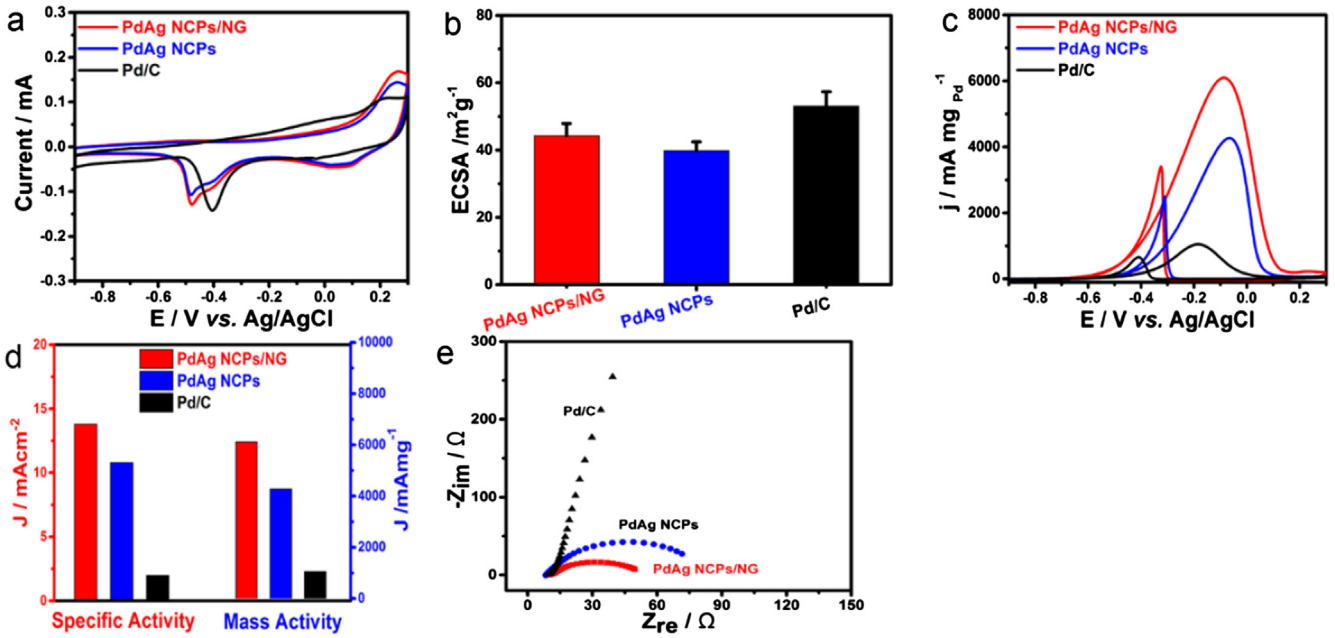

Fig. 4. CV curves of PdAg NCPs/NG, PdAg NCPs, and commercial Pd/C catalysts performed in (a) 1 M KOH solution and (c) 1 M KOH + 1 M EG solution at the scan rate of 50 mV s^{-1}. The corresponding histrograms for (b) ECSAs and (d) electrocatalytic activities of different catalysts toward EGOR. (e) Nyquist plots of different catalysts performed in 1 M KOH + 1 M EG solution at the potential of −0.15 V.

While the PdAg NCPs and commercial Pd/C exhibit relatively apparent change in CV curves with 64.4% and 76.5% losses in electrocatalytic activities (Fig. 6), further confirming the better long-term stability of PdAg NCPs/NG. The newly-constructed PdAg NCPs/NG display outstanding electrocatalytic activity and durability in comparison with PdAg/NCPs and Pd/C catalysts, which can be

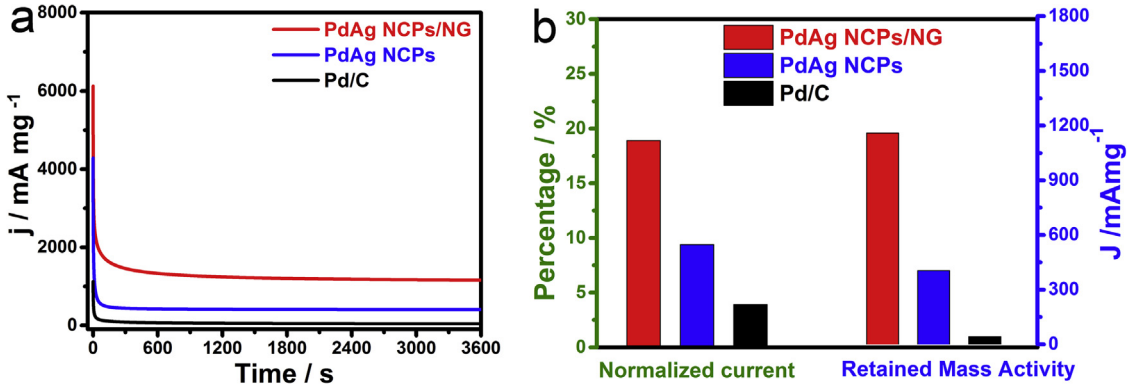

Fig. 5. (a) CA curves of PdAg NCPs/NG, PdAg NCPs, and commercial Pd/C catalysts performed in 1 M KOH + 1 M EG solution at the fixed potential of −0.15 V for 3600 s. (b) The corresponding normalized current percentage and retained mass activies of different catalysts after CA tests.

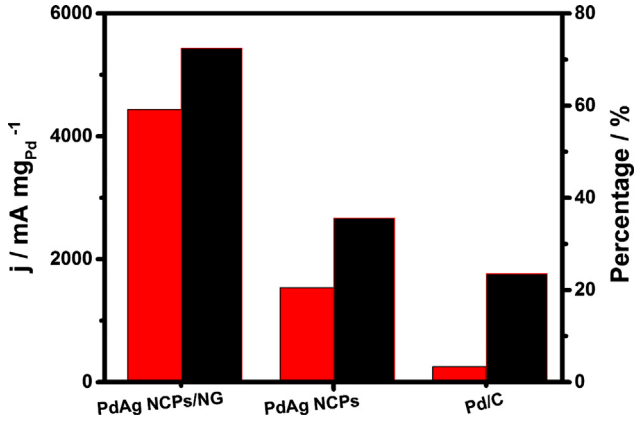

Fig. 6. Histogram of retained mass activities and normalized current percentage of PdAg NCPs/NG, PdAg NCPs, and commercial Pd/C after continous CVs of 500 cycles.

attributed to the unique highly open capsule-like nanostructure with more surface active areas [48], the strong synergistic effects between Pd and Ag [49], as well as the successful introduction of NG support [28,50,51].

4. Conclusions

In summary, we have successfully engineered an advanced class of NG-supported PdAg NCPs catalysts via a facile one-pot strategy, which can serve as an efficient electrocatalysts for EGOR. Owing to the highly open nanostructure, high surface active areas, strong synergistic effects between Pd and Ag, the resultant PdAg NCPs/NG exhibit notable EGOR activity with the mass and specific activities of 6118.3 mA mg^{-1} and 13.8 mA cm^{-2}, respectively, both of which are much higher than those of PdAg NCPs and commercial Pd/C catalysts. More significantly, due to the successful introduction of NG support, the resultant PdAg NCPs/NG also display remarkably improved electrocatalytic durability, which can maintain the electrocatalytic activity of 72.5% for at least 500 potential cycles, showing enormous potential for industrial applications. We expect this work will inspire more researchers to focus on the construction of well-defined and cost-efficient nanocatalysts for the practical applications of fuel cells.

Acknowledgements

This work was sponsored by K.C. Wong Magna Fund in Ningbo University. This work was also supported by the Open Project Program of the State Key Laboratory of Photocatalysis on Energy and Environment (Grant SKLPEE-KF201808), Fuzhou University. The authors also appreciate to the National Natural Science Foundation of China (Grant 21603111, 51702173, 41522304, and 21577142).

Appendix A. Supplementary material

Supplementary data to this article can be found online at https://doi.org/10.1016/j.jcis.2018.10.003.

References

[1] M. Zhu, S. Kim, L. Mao, M. Fujitsuka, J. Zhang, X. Wang, T. Majima, Metal-free photocatalyst for H_2 evolution in visible to near-infrared region: black phosphorus/graphitic carbon nitride, J. Am. Chem. Soc. 139 (2017) 13234–13242.
[2] L. Bu, Q. Shao, E. Bin, J. Guo, J. Yao, X. Huang, PtPb/PtNi intermetallic core/atomic layer shell octahedra for efficient oxygen reduction electrocatalysis, J. Am. Chem. Soc. 139 (2017) 9576–9582.
[3] J. Zhang, M. Chen, H. Li, Y. Li, J. Ye, Z. Cao, M. Fang, Q. Kuang, J. Zheng, Z. Xie, Stable palladium hydride as a superior anode electrocatalyst for direct formic acid fuel cells, Nano Energy 44 (2018) 127–134.
[4] H. Zhang, Y. Shang, J. Zhao, J. Wang, Enhanced electrocatalytic activity of ethanol oxidation reaction on palladium-silver nanoparticles via removable surface ligands, ACS Appl. Mater. Interf. 9 (2017) 16635–16643.
[5] L. Zheng, D. Yang, R. Chang, C. Wang, G. Zhang, S. Sun, Crack-tips enriched platinum-copper superlattice nanoflakes as highly efficient anode electrocatalysts for direct methanol fuel cells, Nanoscale 9 (2017) 8918–8924.
[6] L. Bu, C. Tang, Q. Shao, X. Zhu, X. Huang, Three-dimensional Pd_3Pb nanosheet assemblies: high-performance non-Pt electrocatalysts for bifunctional fuel cell reactions, ACS Catal. 8 (2018) 4569–4575.
[7] L. Bu, S. Guo, X. Zhang, X. Shen, D. Su, G. Lu, X. Zhu, J. Yao, J. Guo, X. Huang, Surface engineering of hierarchical platinum-cobalt nanowires for efficient electrocatalysis, Nat. Commun. 7 (2016) 11850.
[8] J. Liu, G. Xu, B. Liu, J. Zhang, A dendritic core-shell Cu@PtCu alloy electrocatalyst resulting in an enhanced electron transfer ability and boosted surface active sites for an improved methanol oxidation reaction, Chem. Commun. 53 (2017) 7457–7460.
[9] L. Huang, Y. Han, X. Zhang, Y. Fang, S. Dong, One-step synthesis of ultrathin Pt_xPb nerve-like nanowires as robust catalysts for enhanced methanol electrooxidation, Nanoscale 9 (2017) 201–207.
[10] Q. Chen, Z. Cao, G. Du, Q. Kuang, J. Huang, Z. Xie, L. Zheng, Excavated octahedral Pt-Co alloy nanocrystals built with ultrathin nanosheets as superior multifunctional electrocatalysts for energy conversion applications, Nano Energy 39 (2017) 582–589.
[11] Y. Ma, L. Yin, T. Yang, Q. Huang, M. He, H. Zhao, D. Zhang, M. Wang, Z. Tong, One-pot synthesis of concave platinum-cobalt nanocrystals and their superior catalytic performances for methanol electrochemical oxidation and oxygen electrochemical reduction, ACS Appl. Mater. Interf. 9 (2017) 36164–36172.
[12] Z.N. Yu, Z. Zhang, Z.S. Lv, M.T. Liu, L. Zhang, A.J. Wang, L.Y. Jiang, J.J. Feng, Platinum69-cobalt31 alloyed nanosheet nanoassemblies as advanced bifunctional electrocatalysts for boosting ethylene glycol oxidation and oxygen reduction, J. Colloid Interf. Sci. 525 (2018) 216–224.
[13] L.Y. Zhang, Z. Liu, Graphene decorated with Pd_4Ir nanocrystals: ultrasound-assisted synthesis, and application as a catalyst for oxidation of formic acid, J. Colloid Interf. Sci. 505 (2017) 783–788.
[14] M. Wang, Z. Ma, R. Li, B. Tang, X.-Q. Bao, Z. Zhang, X. Wang, Novel flower-like PdAu(Cu) anchoring on a 3D rGO-CNT sandwich-stacked framework for highly efficient methanol and ethanol electro-oxidation, Electrochim. Acta 227 (2017) 330–344.

[15] S.S. Chen, Z.Z. Yang, A.J. Wang, K.M. Fang, J.J. Feng, Facile synthesis of bimetallic gold-palladium nanocrystals as effective and durable advanced catalysts for improved electrocatalytic performances of ethylene glycol and glycerol oxidation, J. Colloid Interf. Sci. 509 (2018) 10–17.
[16] D. Chen, P. Sun, H. Liu, J. Yang, Bimetallic Cu–Pd alloy multipods and their highly electrocatalytic performance for formic acid oxidation and oxygen reduction, J. Mater. Chem. A 5 (2017) 4421–4429.
[17] Q. Xue, G. Xu, R. Mao, H. Liu, J. Zeng, J. Jiang, Y. Chen, Polyethyleneimine modified AuPd@PdAu alloy nanocrystals as advanced electrocatalysts towards the oxygen reduction reaction, J. Energy Chem. 26 (2017) 1153–1159.
[18] S.H. Han, J. Bai, H.M. Liu, J.H. Zeng, J.X. Jiang, Y. Chen, J.M. Lee, One-pot fabrication of hollow and porous Pd-Cu alloy nanospheres and their remarkably improved catalytic performance for hexavalent chromium reduction, ACS Appl. Mater. Interf. 8 (2016) 30948–30955.
[19] W. Wang, Y. Yang, Y. Liu, F. Wang, Y. Kang, Z. Lei, Dealloyed different atom ratios $Pd_x(FeCo)_{10-x}$ nanoparticle: promising electrocatalyst towards ethylene glycol oxidation, Int. J. Hydrogen Energy 41 (2016) 300–306.
[20] W. Niu, Y. Gao, W. Zhang, N. Yan, X. Lu, Pd-Pb alloy nanocrystals with tailored composition for semihydrogenation: taking advantage of catalyst poisoning, Angew. Chem. 54 (2015) 8271–8274.
[21] Z.-Z. Yang, L. Liu, A.-J. Wang, J. Yuan, J.-J. Feng, Q.-Q. Xu, Simple wet-chemical strategy for large-scaled synthesis of snowflake-like PdAu alloy nanostructures as effective electrocatalysts of ethanol and ethylene glycol oxidation, Int. J. Hydrogen Energy 42 (2017) 2034–2044.
[22] X. Weng, Q. Liu, J.J. Feng, J. Yuan, A.J. Wang, Dendrite-like PtAg alloyed nanocrystals: highly active and durable advanced electrocatalysts for oxygen reduction and ethylene glycol oxidation reactions, J. Colloid Interf. Sci. 504 (2017) 680–687.
[23] H. Wang, W. Yang, Q. Zhang, Q. Qiu, Shape-controlled synthesis of palladium-copper nanoalloys with improved catalytic activity for ethanol electrooxidation, Int. J. Electrochem. 2016 (2016) 1–8.
[24] L. Zhang, Z. Xie, J. Gong, Shape-controlled synthesis of Au-Pd bimetallic nanocrystals for catalytic applications, Chem. Soc. Rev. 45 (2016) 3916–3934.
[25] D. Chen, P. Sun, H. Liu, J. Yang, Bimetallic Cu–Pd alloy multipods and their highly electrocatalytic performance for formic acid oxidation and oxygen reduction, J. Mater. Chem. A 57 (2017) 4421–4429.
[26] N. Ma, X. Liu, Z. Yang, G. Tai, Y. Yin, S. Liu, H. Li, P. Guo, X.S. Zhao, Carrageenan asissted synthesis of palladium nanoflowers and their electrocatalytic activity toward ethanol, ACS Sustain. Chem. Eng. 67 (2017) 1133–1140.
[27] L. Yu, J.F. Yang, B.Y. Guan, Y. Lu, X.W.D. Lou, Hierarchical hollow nanoprisms based on ultrathin Ni-Fe layered double hydroxide nanosheets with enhanced electrocatalytic activity towards oxygen evolution, Angew. Chem. 57 (2018) 172–176.
[28] L. Sun, B. Liao, X. Ren, Y. Li, P. Zhang, L. Deng, Y. Gao, Ternary PdNi-based nanocrystals supported on nitrogen-doped reduced graphene oxide as highly active electrocatalysts for the oxygen reduction reaction, Electrochim. Acta 235 (2017) 543–552.
[29] D.-X. Yu, A.-J. Wang, L.-L. He, J. Yuan, L. Wu, J.-R. Chen, J.-J. Feng, Facile synthesis of uniform AuPd@Pd nanocrystals supported on three-dimensional porous N-doped reduced graphene oxide hydrogels as highly active catalyst for methanol oxidation reaction, Electrochim. Acta 213 (2016) 565–573.
[30] Y. Zhang, Y. Liu, W. Liu, X. Li, L. Mao, Synthesis of honeycomb-like mesoporous nitrogen-doped carbon nanospheres as Pt catalyst supports for methanol oxidation in alkaline media, Appl. Surf. Sci. 407 (2017) 64–71.
[31] X.-Y. Zhu, Z.-S. Lv, J.-J. Feng, P.-X. Yuan, L. Zhang, J.-R. Chen, A.-J. Wang, Controlled fabrication of well-dispersed AgPd nanoclusters supported on reduced graphene oxide with highly enhanced catalytic properties towards 4-nitrophenol reduction, J. Colloid Interf. Sci. 516 (2018) 355–363.
[32] D. Chanda, A.S. Dobrota, J. Hnát, Z. Sofer, I.A. Pašti, N.V. Skorodumova, M. Paidar, K. Bouzek, Investigation of electrocatalytic activity on a N-doped reduced graphene oxide surface for the oxygen reduction reaction in an alkaline medium, Int. J. Hydrogen Energy 43 (2018) 12129–12139.
[33] X. Peng, D. Chen, X. Yang, D. Wang, M. Li, C.C. Tseng, R. Panneerselvam, X. Wang, W. Hu, J. Tian, Y. Zhao, Microwave-assisted synthesis of highly dispersed PtCu nanoparticles on three-dimensional nitrogen-doped graphene networks with remarkably enhanced methanol electrooxidation, ACS Appl. Mater. Interf. 8 (2016) 33673–33680.
[34] N. Zhang, S. Guo, X. Zhu, J. Guo, X. Huang, Hierarchical Pt/Pt_xPb core/shell nanowires as efficient catalysts for electrooxidation of liquid fuels, Chem. Mater. 28 (2016) 4447–4452.
[35] N. Zhang, L. Bu, S. Guo, J. Guo, X. Huang, Screw thread-like platinum-copper nanowires bounded with high-index facets for efficient electrocatalysis, Nano Lett. 16 (2016) 5037–5043.
[36] P. Wang, X. Zhang, J. Zhang, S. Wan, S. Guo, G. Lu, J. Yao, X. Huang, Precise tuning in platinum-nickel/nickel sulfide interface nanowires for synergistic hydrogen evolution catalysis, Nat. Commun. 8 (2017) 14580.
[37] H. Huang, J. Zhu, D. Li, C. Shen, M. Li, X. Zhang, Q. Jiang, J. Zhang, Y. Wu, Pt nanoparticles grown on 3D RuO_2-modified graphene architectures for highly efficient methanol oxidation, J. Mater. Chem. A 5 (2017) 4560–4567.
[38] C. Peng, Y. Hu, M. Liu, Y. Zheng, Hollow raspberry-like PdAg alloy nanospheres: high electrocatalytic activity for ethanol oxidation in alkaline media, J. Power Sources 278 (2015) 69–75.
[39] D. Bin, B. Yang, K. Zhang, C. Wang, J. Wang, J. Zhong, Y. Feng, J. Guo, Y. Du, Design of PdAg hollow nanoflowers through galvanic replacement and their application for ethanol electrooxidation, Chem. Eur. J. 22 (2016) 16642–16647.
[40] L. Li, M. Chen, G. Huang, N. Yang, L. Zhang, H. Wang, Y. Liu, W. Wang, J. Gao, A green method to prepare Pd–Ag nanoparticles supported on reduced graphene oxide and their electrochemical catalysis of methanol and ethanol oxidation, J. Power Sources 263 (2014) 13–21.
[41] M. Zhu, C. Zhai, M. Sun, Y. Hu, B. Yan, Y. Du, Ultrathin graphitic C_3N_4 nanosheet as a promising visible-light-activated support for boosting photoelectrocatalytic methanol oxidation, Appl. Catal. Environ. 203 (2017) 108–115.
[42] Y. Liu, S. Yang, S.-N. Yin, L. Feng, Y. Zang, H. Xue, In situ construction of fibrous AgNPs/g-C_3N_4 aerogel toward light-driven CO_x-free methanol dehydrogenation at room temperature, Chem. Eng. J. 334 (2018) 2401–2407.
[43] C. Zhai, J. Hu, M. Sun, M. Zhu, Two dimensional visible-light-active Pt-BiOI photoelectrocatalyst for efficient ethanol oxidation reaction in alkaline media, Appl. Surf. Sci. 430 (2018) 578–584.
[44] M. Sun, J. Hu, C. Zhai, M. Zhu, J. Pan, A p-n heterojunction of CuI/TiO_2 with enhanced photoelectrocatalytic activity for methanol electro-oxidation, Electrochim. Acta 245 (2017) 863–871.
[45] D. Qazzazie, O. Yurchenko, S. Urban, J. Kieninger, G. Urban, Platinum nanowires anchored on graphene-supported platinum nanoparticles as a highly active electrocatalyst towards glucose oxidation for fuel cell applications, Nanoscale 9 (2017) 6436–6447.
[46] S. Fu, C. Zhu, J. Song, P. Zhang, M.H. Engelhard, H. Xia, D. Du, Y. Lin, Low Pt-content ternary PdCuPt nanodendrites: an efficient electrocatalyst for oxygen reduction reaction, Nanoscale 9 (2017) 1279–1284.
[47] V. Beermann, M. Gocyla, S. Kuhl, E. Padgett, H. Schmies, M. Goerlin, N. Erini, M. Shviro, M. Heggen, R.E. Dunin-Borkowski, D.A. Muller, P. Strasser, Tuning the electrocatalytic oxygen reduction reaction activity and stability of shape-controlled Pt-Ni nanoparticles by thermal annealing - elucidating the surface atomic structural and compositional changes, J. Am. Chem. Soc. 139 (2017) 16536–16547.
[48] C. Hu, X. Zhai, Y. Zhao, K. Bian, J. Zhang, L. Qu, H. Zhang, H. Luo, Small-sized PdCu nanocapsules on 3D graphene for high-performance ethanol oxidation, Nanoscale 6 (2014) 2768–2775.
[49] M. Liu, Y. Lu, W. Chen, PdAg nanorings supported on graphene nanosheets: highly methanol-tolerant cathode electrocatalyst for alkaline fuel cells, Adv. Funct. Mater. 23 (10) (2013) 1289–1296.
[50] M. Li, Q. Jiang, M. Yan, Y. Wei, J. Zong, J. Zhang, Y. Wu, H. Huang, Three-dimensional boron- and nitrogen-codoped graphene aerogel-supported Pt nanoparticles as highly active electrocatalysts for methanol oxidation reaction, ACS Sustain. Chem. Eng. 6 (2018) 6644–6653.
[51] H. Huang, J. Zhu, W. Zhang, C.S. Tiwary, J. Zhang, Xin Zhang, Q. Jiang, H. He, Y. Wu, W. Huang, P.M. Ajayan, Q. Yan, Controllable codoping of nitrogen and sulfur in graphene for highly efficient Li-oxygen batteries and direct methanol fuel cells, Chem. Mater. 28 (2016) 1737–1745.